Semiconductor Nanocrystals: A Powerful Visual Aid for Introducing the Particle in a Box

Tadd Kippeny, Laura A. Swafford, and Sandra J. Rosenthal*
Department of Chemistry, Vanderbilt University, Nashville, TN 37235; *sjr@femto.cas.vanderbilt.edu

Physical chemistry is an intimidating subject for many students, especially those who have an aversion to mathematics. For these students it is important to provide visual demonstrations of difficult concepts, lest they become frustrated and lost in a sea of equations. Several curriculum reform groups have also advocated the importance of placing course content in the context of real scientific, societal, or technological problems (*1*). Many of these efforts have focused on introductory chemistry courses. While physical chemistry students are more advanced, students at all levels appreciate the connection between course content and the world they encounter outside of the classroom. Quantum mechanics is unlike thermodynamics (engines, refrigeration) and kinetics (catalysis, enzymes); it is difficult for students to see the "real world" significance of quantum mechanics or to visualize quantum mechanical phenomena. With the advent of nanotechnology, the construction of devices on a nanometer scale, it is not only possible but important to connect quantum mechanical course content with technological problems.

Semiconductor nanocrystals, nanoscale building blocks for new materials and technologies (*2*), provide a means for connecting lecture content in quantum mechanics to real-world technological problems. Nanocrystals can also be incorporated into freshman chemistry lectures, where atomic spectroscopy is introduced, and into inorganic chemistry, where organometallic synthesis, ligand field theory, and group theory are discussed.

The "particle in a box" is often the first problem students encounter in their studies of quantum mechanics. The series of CdSe nanocrystals shown in Figure 1 is a powerful visual demonstration of the particle in a box. These nanocrystals were chemically synthesized to have a desired size. They have the same wurtzite crystal structure as bulk CdSe, but consist of only a few hundred to a few thousand atoms (Figures 2 and 3). As the nanocrystal size increases, the energy of the first excited state decreases, qualitatively following particle-in-a-box behavior (Figure 4).

This size dependence and the emergence of discrete electronic states from the continuum of levels in the valence and conduction bands of the bulk semiconductor result from quantum confinement; hence semiconducting nanocrystals are also referred to as "quantum dots". In bulk CdSe, the electron–hole pair created upon absorption of a photon maintains a characteristic distance known as the bulk Bohr exciton radius. CdSe has a Bohr exciton radius of ~56 Å *(3),* so for nanocrystals smaller than 112 Å in diameter the electron and hole cannot achieve their desired distance and become particles trapped in a box. The discrete electronic transitions that emerge from the continuum can be labeled as atomic transitions (*4*). Because the energy of these transitions can be tuned by size, nanocrystals have also earned the nickname of "artificial atoms".

This article provides an overview of methods by which nanocrystals can be prepared and describes in detail the preparation of CdSe nanocrystals by the pyrolysis of organometallic precursors. It then discusses the energy shift of CdSe nanocrystals with size and surveys some applications of nanocrystals.

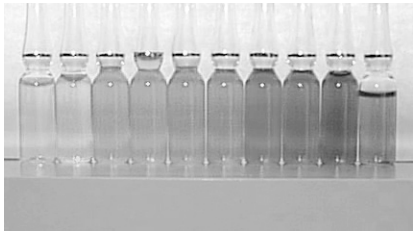

Figure 1. CdSe nanocrystals dissolved in toluene. The size of the nanocrystals progressively increases from 19 Å on the left to 60 Å on the right. A color version of this figure is shown on p 1027.

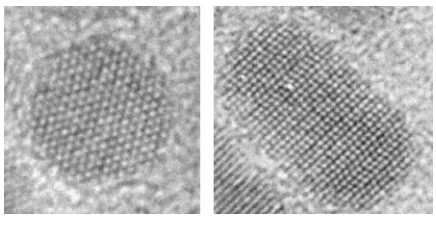

Figure 2. Transmission electron micrograph of single CdSe nanocrystals viewed looking (left) down the C_{3v} axis and (right) parallel to the C_{3v} axis.

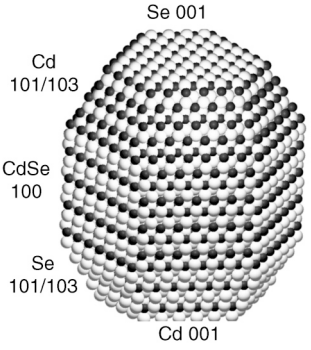

Figure 3. Model of a wurtzite CdSe nanocrystal. This model was constructed from transmission electron micrographs such as those in Figure 2.

Nanocrystal Fabrication

Semiconductor nanocrystals can be fabricated by a variety of methods, including vapor deposition, ion implantation, sol–gel methods, micelle methods, and organometallic synthesis. Vapor deposition techniques for the growth of quantum dots, including atomic-vapor deposition and chemical-vapor deposition, rely on a lattice mismatch between the deposited substance and a crystalline substrate. The lattice mismatch induces strain, which is relieved by cluster formation. An example is Ge deposition on Si, which leads to the formation of Ge pyramids. Repeating the deposition of Si and Ge into a multilayer film enhances the regularity in position and size of the quantum dots in a "self-organized" way (*5, 6*). The resulting three-dimensional structure of dots could potentially communicate electronically but without wires.

In the ion implantation technique for forming nanocrystals, the host matrix, for example crystalline SiO_2, first undergoes a blanket implant of one of the elements, for example As. A high-energy ion beam is then used to implant the second element, for example Ga. Implantation creates a supersaturated solution of an impurity in the near surface region, and thermal annealing leads to precipitation and a broad size distribution of nanocrystals. Recent developments using a finely focused ion beam overcome this size distribution limitation at the expense of a substantial increase in time for fabrication. The spot size for the finely focused ion beam can be as small as 70 Å, and thermally induced atomic clustering can result in crystallites of considerably smaller size.

Sol–gel methods for fabricating nanocrystals also result in quantum dots that are embedded in a matrix. A variety of nanocomposites have been synthesized by this technique (*7*). One example is a cadmium sulfide–silica gel nanocomposite. Cadmium nitrate is dissolved in conventional sol–gel formulations using tetraethylorthosilicate. This is followed by reaction with dihydrogen sulfide. The resulting particles vary in size from 16 to 100 Å, depending upon the weight percentage of CdS in the silica gel and the conditions of thermal annealing. The sol gel can be processed as a porous ceramic xerogel of high surface area, which can serve as a catalytic support. Here the CdS particles could catalyze CO_2 fixation (*8*). Alternatively the sol–gel solution could be spun into an optical fiber. For instance, a fiber containing PbS particles could be used for nonlinear optics.

The micelle method of fabricating nanocrystals is perhaps the most approachable for the undergraduate laboratory. A method for the synthesis of CdS nanocrystals has been developed by Vossmeyer et al. (*9*). A cadmium salt is dissolved in a thioglycerol–water solution whose pH is adjusted to 11.2 before the addition of dihydrogen sulfide with vigorous stirring. The particle size is controlled by the amount of dihydrogen sulfide added as well as the temperature and duration of further heating. To improve the size distribution, the samples are size-selectively precipitated.

The synthesis of nanocrystals by the pyrolysis of organometallic reagents, first developed by Murray et al. (*10*), is the best chemical procedure for producing large quantities of II-VI and III-V quantum dots in a processable form, with a narrow size distribution and with no vacancies in the nanocrystal. The method used to prepare the CdSe nanocrystals displayed in Figure 1 is outlined in Figure 5 (*10, 11*).[1] First stock solutions of the Cd and Se precursors are prepared and stored in a glove box. Ten milliliters of $Cd(CH_3)_2$ is vacuum transferred to a 25-mL round-bottom flask on a Schlenk line and then immediately transferred to the glove box while maintaining vacuum, as $Cd(CH_3)_2$ is pyrophoric.[2] A 0.96-g portion of Se powder is complexed with 100 mL of tributylphosphine (TBP) and this solution is stored in the box until use. Just before the reaction, 166 µL of $Cd(CH_3)_2$ is mixed with 10 mL of the Se–TBP solution. This solution degrades with time and cannot be stored. The organocadmium and selenium reagents are injected via a large-bore syringe into 12 g of trioctylphosphine oxide (TOPO) at 360 °C, and nanocrystal nucleation occurs (Warning: 360 °C is above the flash point of TOPO, and this reaction must be done under inert atmosphere). The temperature of the reaction mixture

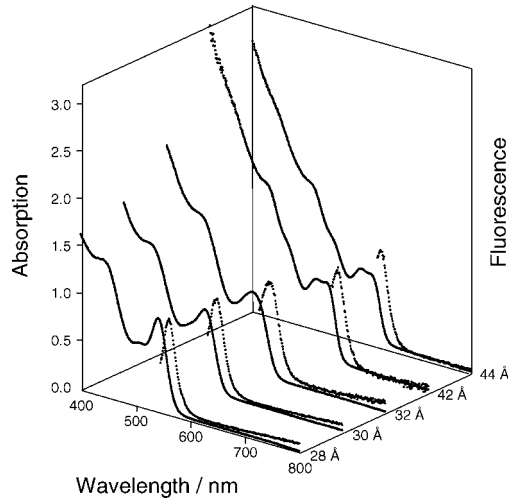

Figure 4. Absorption and emission spectra of CdSe nanocrystals. As the size of the nanocrystal increases both the absorption and emission shift to higher wavelengths.

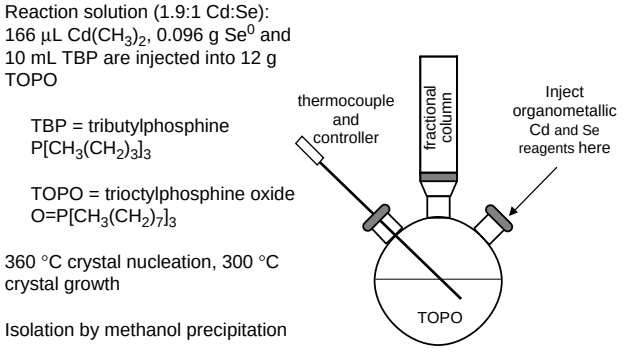

Figure 5. Procedure for synthesizing high-quality, monodisperse CdSe nanocrystals by the pyrolysis of organometallic precursors. This open-atmosphere setup is designed to be used in a glove box. The reaction can be performed outside a glove box under argon.

is immediately reduced to 300 °C, allowing the nanocrystals to grow to the desired size, at which point the reaction is stopped by removing the heating mantle from the reaction vessel. The vials in Figure 1 show a range of growth times from 0 minutes (19 Å, furthest left) to 3 hours (60 Å, furthest right). The TOPO ligands bind to surface Cd atoms, giving the nanocrystals an organic shell and providing solubility in organic solvents and polymers. The size distribution of these nanocrystals is ±2 Å.

Energy Shift and Nanocrystal Size

The most immediately obvious evidence of quantum confinement in semiconductor nanocrystals is the shift in the optical absorption and emission spectra with size. An absorption event promotes an electron from the valence band to the conduction band, leaving a region of positive charge (the "hole") behind in the valence band. The resultant bound electron–hole pair is an excellent real-world example of the particle-in-a-box model in quantum mechanics, and a basic model for the behavior of this system was developed by L. E. Brus (*12, 13*). To explain the behavior of the electron and hole in this system, Brus's model makes the following approximations of the system:

1. The nanocrystal is spherical, with a radius of R.
2. The interior of the nanocrystal is a uniform medium; there are no point charges or occupied spaces other than the excited electron and hole (i.e., nuclei or bound electrons).
3. The potential energy outside the nanocrystal is infinite; thus the electron and hole are always found within the nanocrystal (i.e., the surface of the nanocrystal defines the walls of the "box").

Using CdSe nanocrystals as an example, we first explore the behavior of a single charged particle within a nanocrystal. The Hamiltonian for a free point charge in a nanocrystal is

$$\mathcal{H} = -\frac{h^2}{8\pi^2 m_c}\nabla_c^2 + \hat{V}; \quad \hat{V} = \begin{cases} 0, & r \le R \\ \infty, & r \ge R \end{cases} \tag{1}$$

where m_c is the effective mass of the point charge and r is the distance from the center of the nanocrystal. The solution to the Schrödinger equation in this case is the familiar particle-in-a-box solution to the Schrödinger equation, modified for the case of a sphere:

$$\psi_n(r) = \frac{1}{r\sqrt{2\pi R}}\sin\left(\frac{n\pi r}{R}\right) \tag{2}$$

$$E_n = \frac{h^2 n^2}{8 m_c R^2}; \quad n = 1, 2, 3, \ldots \tag{3}$$

Qualitatively, eq 3 illustrates the particle-in-a-box behavior of nanocrystals. As the size of the nanocrystal increases, the absorption energy decreases. In reality, creation of an exciton in a nanocrystal involves two charges, the electron and the hole. Nevertheless, as we shall see below, the predominant energy feature for the excitation also follows particle-in-a-box behavior.

In the case of an electron–hole pair, the Hamiltonian is

$$\mathcal{H} = -\frac{h^2}{8\pi^2 m_e}\nabla_e^2 - \frac{h^2}{8\pi^2 m_h}\nabla_h^2 + \hat{V}(\bar{S}_e, \bar{S}_h) \tag{4}$$

where $\bar{S}_e$ and $\bar{S}_h$ are the positions of the electron and hole, respectively, within the nanocrystal, $m_e = 0.13m_0$ is the effective mass of the electron in CdSe (m_0 is the free-electron mass), and $m_h = 0.45m_0$ is the effective mass of the hole (*15*). Here the potential energy $\hat{V}(\bar{S}_e,\bar{S}_h)$ consists of two parts and is still assumed infinite for $r > R$. For $r < R$ the first part is the Coulomb attraction between the negatively charged electron and the positively charged hole:

$$\hat{V}_{Coul}(\bar{S}_e, \bar{S}_h) = -\frac{e^2}{4\pi\varepsilon_{CdSe}\varepsilon_0|\bar{S}_e - \bar{S}_h|} \tag{5}$$

where ε_{CdSe} is 10.6, the dielectric constant for bulk CdSe (*15*), and ε_0 is the vacuum permittivity. The second component of the potential energy is the polarization energy. Essentially, a point charge inside a nanocrystal polarizes the crystal. This polarization affects the energy of the second charge. The polarization term is given by

$$\hat{V}_{pol}(\bar{S}_e, \bar{S}_h) = \frac{e^2}{2}\sum_{k=1}^{\infty}\alpha_k\frac{S_e^{2k} + S_h^{2k}}{R^{2k+1}} \tag{6}$$

where

$$\alpha_k = \frac{(\varepsilon - 1)(k+1)}{4\pi\varepsilon_{CdSe}\varepsilon_0(\varepsilon k + k + 1)}; \quad \varepsilon = \frac{\varepsilon_{CdSe}}{\varepsilon_{out}} \tag{7}$$

and ε_{out} is the dielectric constant of the medium surrounding the nanocrystal. Combining eqs 4–7, the total Hamiltonian for the electron–hole system in a nanocrystal is

$$\mathcal{H} = -\frac{h^2}{8\pi^2 m_e}\nabla_e^2 - \frac{h^2}{8\pi^2 m_h}\nabla_h^2 - \frac{e^2}{4\pi\varepsilon_{CdSe}\varepsilon_0|\bar{S}_e - \bar{S}_h|} + \frac{e^2}{2}\sum_{k=1}^{\infty}\alpha_k\frac{S_e^{2k} + S_h^{2k}}{R^{2k+1}} \tag{8}$$

From this equation, it is clear that as $R \to \infty$, the polarization term $\hat{V}_{pol}(\bar{S}_e,\bar{S}_h) \to 0$, and the Hamiltonian in eq 8 becomes the hydrogen-like Hamiltonian of the bulk.

To evaluate the lowest energy of the electron-hole system, it is first necessary to determine the wave function $\Phi(\bar{S}_e,\bar{S}_h)$ for the system. This wave function must be some function of the lowest-energy wave functions of the individual charges within the nanocrystal, $\psi(\bar{S}_e)$ and $\psi(\bar{S}_h)$, as in eq 2. As a first-order approximation we can use the uncorrelated wave function:

$$\Phi_{ex}(\bar{S}_e, \bar{S}_h) = \psi_1(\bar{S}_e)\psi_1(\bar{S}_h) \tag{9}$$

Using this wave function and the Hamiltonian in eq 8, and solving the Schrödinger equation, the calculated internal energy of the exciton is

$$E_{ex} = \frac{h^2}{8R^2}\left(\frac{1}{m_e} + \frac{1}{m_h}\right) - \frac{1.8e^2}{4\pi\varepsilon_{CdSe}\varepsilon_0 R} + \frac{e^2}{R}\overline{\sum_{k=1}^{\infty}\alpha_k\left(\frac{S}{R}\right)^{2k}} \tag{10}$$

Here

$$\left|\overline{\bar{S}_e - \bar{S}_h}\right| = \frac{R}{1.8}$$

is the average separation of the two charges, and as the electron and hole are confined to the same space, the S_e and S_h terms in the polarization potential of eq 8 are collapsible into a single positional term. The bar over this term denotes the average over the wave function $\psi_1(\bar{S})$:

$$E_{pol} = \frac{e^2}{R}\overline{\sum_{k=1}^{\infty} \alpha_k \left(\frac{S}{R}\right)^{2k}} = \frac{e^2(\varepsilon - 1)}{2\pi R^2 \varepsilon_{CdSe}\varepsilon_0}\int_{r=0}^{R} \sin^2\left(\frac{\pi r}{R}\right)\sum_{k=1}^{\infty}\frac{k+1}{(\varepsilon+1)k+1}\left(\frac{r}{R}\right)^{2k} dr \quad (11)$$

As E_{pol} is small compared to the kinetic and Coulomb energies, a good understanding of the lowest-energy excitonic state may be made by omitting this term. Alternately, because $(r/R)^{2k} \to 0$ rapidly as $k \to \infty$, the polarization term may be truncated. Standard mathematical evaluation programs such as Maple and Mathematica are capable of evaluating the polarization energy for the truncation k: $1 \to 10$, which is a good approximation of E_{pol} obtained using the full sum. Figure 6 shows the dependence of $E_{pol}R$ on ε for CdSe using a truncated sum.

In eq 10 the predominant energy term, particularly at small R, is the first term, the kinetic energy. The form of this energy is simply the sum of the energies of two particles in one box. Thus the size dependence of the first absorption and emission features of the nanocrystal can be linked to the particle-in-a-box model.

To compare the theoretical energy with experiment, we can look at the energy needed to create the lowest-energy exciton:

$$E_{tr} = E_g + E_{ex} \quad (12)$$

where E_{tr} is the transition energy, and E_g is 1.751 eV, the bulk band gap of CdSe (*14*). Figure 7 compares the transition energy calculated using Brus's model with experimental results correlating transmission electron microscopy sizing of nanocrystals with absorption spectroscopy of the first absorption peak (Alivisatos group, private communication). Although the calculated transition energies match experimental results very closely for large R, they deviate significantly from experimental values at small R. It is possible to obtain better quantitative agreement by including the prolate elliptical shape of the nanocrystal, the effect of the wurtzite crystal structure on the valence band energy, and by considering a quantum mechanical exchange interaction between the electron and hole, but these are topics for advanced quantum mechanics (*15*). Nevertheless, Brus's model yields energies that are fairly close to experimental values for larger nanocrystals and it provides an excellent understanding of the behavior of lowest-energy excitons using basic quantum mechanical principles.

Applications of Semiconductor Nanocrystals

A variety of applications have been demonstrated for nanocrystals, including tunable light emitting diodes (LEDs) (*16–20*), photovoltaics (*21, 22*), single-electron transistors (*23, 24*), and fluorescent tags for biological imaging applications (*25–27*). All of these applications result from the particle-in-a-box-like properties of nanocrystals, making them an ideal teaching tool for connecting quantum mechanics to real-world applications. These applications are discussed briefly below.

Light-emitting diodes based on organic materials (polymers or small molecules) have generated much interest for large-area, flat-panel display applications. These devices use either an electron-transporting emitting layer and a hole-transporting layer or a separate emissive layer sandwiched between electron- and hole-transport layers. When a bias is applied across the electrodes, injected electrons and holes radiatively recombine in the emissive layer. The color of the electroluminescence is dictated by the emitting molecule. It is difficult to tune the color of these devices for two reasons. First, the emission spectrum of organic molecules is broad, lowering the spectral purity of the device. Second, different molecules have to be synthesized to obtain different emitting colors. Semiconductor nanocrystals offer an attractive alternative. The emission spectrum of nanocrystals is very narrow (spectrally pure) and

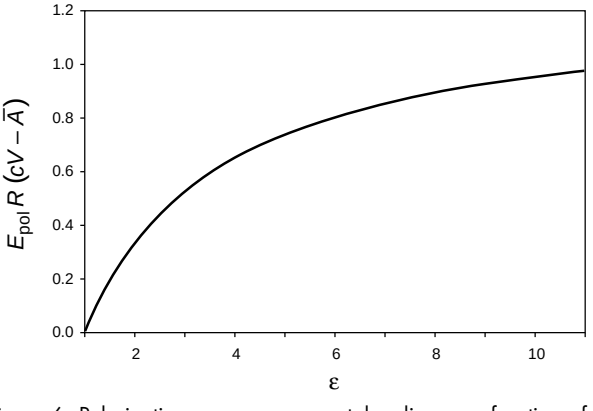

Figure 6. Polarization energy nanocrystal radius as a function of ε. This graph was made according to eq 11, using a truncated sum k: $1 \to 10$. If ε and R are known, then the polarization energy can be found by dividing the appropriate y-axis value by R.

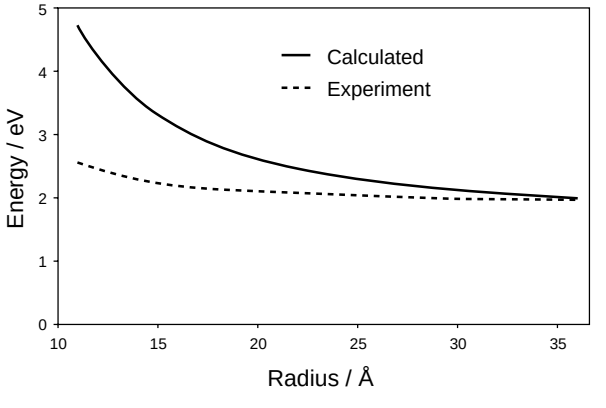

Figure 7. First excitonic transition energy as a function of nanocrystal radius for CdSe. Calculated values were calculated according to eqs 10–12 for a nanocrystal in a vacuum ($\varepsilon_{out} = 1$). These energies are in good agreement with experimental values (Alivisatos group, private communication), but diverge for smaller nanocrystals.

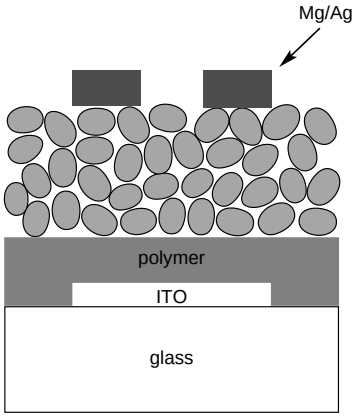

Figure 8. Schematic of a nanocrystal-based light emitting diode (*17*). Positive charges are injected at the transparent, conducting indium tin oxide electrode; negative charges are injected at the magnesium–silver electrode. The charges recombine in the nanocrystals, resulting in the emission of photons. The size of the nanocrystal dictates the color of the electroluminescence.

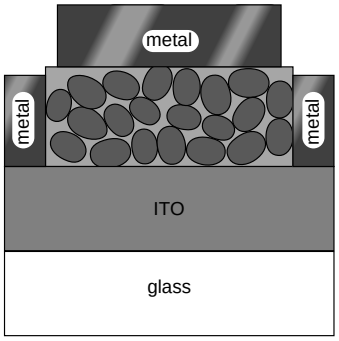

Figure 9. Schematic of a nanocrystal and polymer heterojunction solar cell. Both the polymer and the nanocrystals generate electron–hole pairs upon excitation by light. Electrons travel through the nanocrystals to the aluminum electrode, and holes travel through the polymer to reach the indium tin oxide (ITO) electrode.

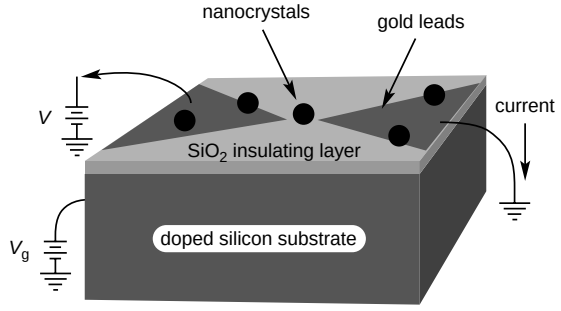

Figure 10. Schematic of a nanocrystal single-electron transistor. As the voltage to the gate (V_g) is increased, conductance across the nanocrystal turns on.

the color of the emission is simply tuned by changing the size of the nanocrystal used in the device. A schematic of a nanocrystal LED is shown in Figure 8. Electrons are injected into the nanocrystals and holes are injected into the polymer. The electrons and holes recombine in the nanocrystals, and the color of the electroluminescence is dictated by the size of the nanocrystals used in the device. Semiconductor nanocrystals have the additional benefit of being more robust than their organic counterparts.

A device structure similar to the LEDs is incorporated for using nanocrystals in solar cells (Figure 9). Here the nanocrystals are directly blended with a polymer that transports positive charge. The nanocrystal harvests sunlight, generating an electron–hole pair in the nanocrystal. The hole is transported by the polymer to a transparent indium tin oxide (ITO) electrode, and the electron hops from nanocrystal to nanocrystal, making its way to an aluminum electrode. The difference in work function between the two electrodes creates an internal electric field, which causes net charge migration. While nanocrystal-based photovoltaics offer the benefits of low-cost, large-area fabrication, their efficiencies are currently much too low for them to be commercially viable. This is because of electron and hole recombination losses. Research is underway to build device structures that more efficiently funnel electrons and holes to their respective electrodes.

A different application of semiconductor nanocrystals is in molecular electronics, the construction of electronic devices on the molecular length scale. Figure 10 shows a schematic of a single-electron transistor composed of a nanocrystal between two gold leads. The gold is coated with hexanedithiol in order to attach the nanocrystal (the sulfur atoms bind both to the gold and to surface Cd atoms of the nanocrystal). As the voltage applied to the gate (the silicon substrate) is increased conductance across the nanocrystal turns on.

Recently it was demonstrated that a special type of nanocrystal, a "core/shell", can be used for fluorescent tags in biological applications. Here a core of one semiconductor nanocrystal is wrapped in a shell of a second semiconductor material (Figure 11). A biologically active molecule is then coordinated to the surface of the core-shell crystal. These nanocrystals have several advantages over organic molecules as fluorescent labels, including resistance to photodegradation, improved brightness, nontoxicity, and size-dependent, narrow emission spectra that enable the simultaneous monitoring of several processes. Additionally, their absorption spectra are continuous above the band gap so that any standard excitation source can be used to simultaneously excite the different sizes of nanocrystals. As an illustration of fluorescence labeling with fluorescent quantum dots, Figure 12 shows drug-conjugated core/shell nanocrystals bound to the serotonin 2A receptor protein on the surface of rat 3T3 cells (P. Gresch, I. Tomlinson, E. Saunders-Bush, S. J. Rosenthal, unpublished work). These nanoconjugates are designed to target only this protein. By linking drugs that have a high affinity and selectivity for specific proteins to the surface of different sizes of core shell nanocrystals, the distribution of different proteins on the surface of living cells can be imaged simultaneously.

All of the applications described above result from the size-tunable optical and electrical properties of semiconductor nanocrystals, which in turn originate from particle-in-a-box-

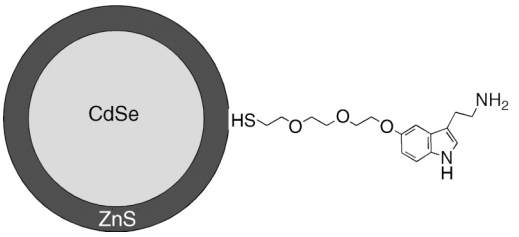

Figure 11. A CdSe–ZnS core–shell nanocrystal labeled with the neurotransmitter serotonin (P. Gresch, I. Tomlinson, E. Saunders-Busch, and S. J. Rosenthal, unpublished). The CdSe core has a narrower band gap than the ZnS shell. Therefore when the CdSe core is excited the electron–hole pair remains relatively confined in the core and the electron and hole radiatively recombine, yielding a highly fluorescent nanocrystal.

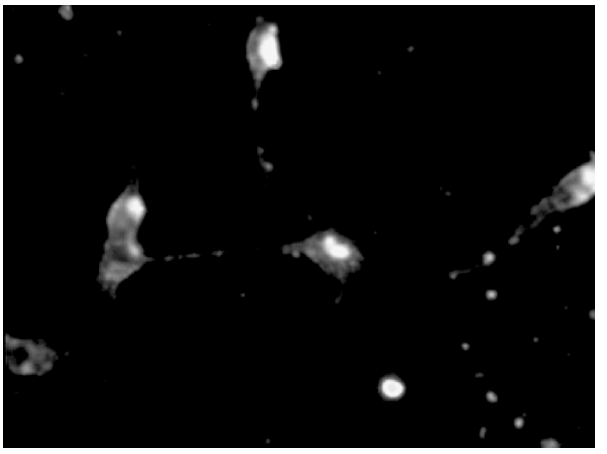

Figure 12. Upon excitation with a UV lamp, core–shell nanocrystals coated with a drug that binds exclusively to the serotonin 2A receptor protein on the surface of rat 3T3 cells fluoresce, showing the locations of these proteins (P. Gresch, I. Tomlinson, E. Saunders-Busch, and S. J. Rosenthal, unpublished). Multiple colors of core–shell nanocrystals could be coated with different drugs, allowing the imaging of several proteins at once with a single light source.

like quantum confinement. Hence nanocrystals provide a beautiful illustration of qualitative particle-in-a-box-like behavior with real-world applications.

Acknowledgments

S. J. Rosenthal is supported by a National Science Foundation CAREER award. T. Kippeny and L. Swafford acknowledge GAANN Fellowships.

Notes

1. A step-by-step procedure for making CdSe nanocrystals can be found at our Web site: *http://www.vanderbilt.edu/AnS/Chemistry/lsms/*.

2. Dimethyl cadmium might be expected to have a similar toxicity (LD_{50}) to dimethyl mercury, which killed Professor Karen Wetterhahn at Dartmouth. Fortunately for those who work with dimethyl cadmium there are two major reasons why it is actually much less toxic. First, cadmium is bound by the scavenging enzyme metallothionein. The bound cadmium is stored in the liver until cell death and then transported to the kidney for life. This explains the low time-weighted average (TWA) for cadmium compounds in the MSDS. Even though $CdMe_2$ may cross the blood–brain barrier it is bioactive; therefore the mechanisms already in place within the body for dealing with heavy metals are effective. Alkyl mercury compounds, in contrast, have no removal mechanism and stay to do damage in the brain. As with any heavy metal there will be illness and possible death from a large acute dose. Concentrations over 0.96 g per kilogram of body mass have toxic effects as cadmium begins to replace copper and zinc in various metallozymes, rendering them inactive (e.g., cytochrome P60 and DNA binding proteins). The second reason dimethyl cadmium is less toxic than expected is that an oversight in early testing over-predicted cadmium toxicity. In testing cadmium as an alternative for the anticorrosive tin in "tin cans", cadmium was found to have a very low LD_{50}. Later work, however, showed that the chicken embryos used for testing overproduced metallothionein, which led to a copper deficiency and fetal death. So although dimethyl cadmium is not as toxic as dimethyl mercury, it is advisable to use a handling program in accordance with exposure, as should practiced when handling any heavy metal (e.g., meticulous glove use and yearly screening required for heavy users). Finally, an inhalation hazard exists. Like any fine particulate, in large doses the fine CdO particles from the rapid degradation of $Cd(CH_3)_2$ in air can cause respiratory distress or failure. Inhalation symptoms usually appear within 1–8 hours of exposure. (Edelman, Phillip; Director of Clinical Services and Toxicology, Division of Occupational and Environmental Medicine, 2300 K Street, N.W., Washington, DC 20037; personal communication.)

Literature Cited

1. Projects Supported by the NSF Division of Undergraduate Education. *J. Chem. Educ.* **1995,** *72*, 639–641; ChemLinks Coalition: Making Chemical Connections (Brock Spencer); Sweeping Change in Manageable Units: a Modular Approach for Chemistry Curriculum Reform (C. Bradley Moore); Establishing New Traditions: Revitalizing the Curriculum (John W. Moore).
2. Alivisatos, A. P. *Endeavor* **1997,** *21*, 56–60.
3. Ekimov, A. I.; Hache, F.; Schanneklein, M. C.; Ricard, D.; Flytzanis, C.; Kudryavtsev, I. A.; Yazeva, T. V.; Rodina, A. V.; Efros, A. L. *J. Opt. Soc. Am. B* **1993,** *10*, 100–107.
4. Norris, D. J.; Sacra, A.; Murray, C. B.; Bawendi, M. G. *Phys. Rev. Lett.* **1994,** *72*, 2612–2615.
5. Lagally, M. G. *J. Chem. Educ.* **1998,** *75*, 277.
6. Liu, F.; Lagally, M. G. *Surf. Sci.* **1997,** *386*, 169.
7. Kwiatkowski, K.; Lukehart, C. M. In *Handbook of Nanostructured Materials and Nanotechnology;* Nalwa, H. S., Ed.; Academic: San Diego, 2000.
8. Fujiwara, H.; Hosokawa, H.; Murakoshi, K.; Wada, Y.; Yanagida, S.; Okada, T.; Kobayashi, H. *J. Phys. Chem. B* **1997,** *101*, 8270.
9. Vossmeyer, T.; Katsikas, L.; Giersig, M.; Popovic, I. G.; Diesne, K.; Chemseddine, A.; Eychmuller, A.; Weller, H. *J. Phys. Chem.* **1994,** *98*, 7665.
10. Murray, C. B.; Norris, D. J.; Bawendi, M. G. *J. Am. Chem. Soc.* **1993,** *115*, 8706–8715.
11. Peng, X.; Wickham, J.; Alivisatos, A. P. *J. Am. Chem. Soc.* **1998,** *120*, 5343–5344.

12. Brus, L. E. *J. Chem. Phys*. **1983,** *79*, 5566–5571.
13. Brus, L. E. *J. Chem. Phys*. **1984,** *80*, 4403–4409.
14. *Landolt-Börnstein: Numerical Data and Functional Relationships in Science and Technology,* New Series, Vol. III-17b; Madelung, O., Ed.; Springer: New York. 1982.
15. Efros, A. L.; Rosen, M.; Kuno, M.; Nirmal, M.; Norris, D. J.; Bawendi, M. *Phys. Rev. B* **1996,** *54*, 4843–4856.
16. Colvin, V. L.; Schlamp, M. C.; Alivisatos, A. P. *Nature* **1994,** *370*, 354–357.
17. Schlamp, M. C.; Peng, X. G.; Alivisatos, A. P. *J. Appl. Phys*. **1997,** *82*, 5837–5842.
18. M. C. Schlamp, M. C. Electoluminescence in Semiconductor Nanocrystals; Ph.D. Thesis, University of California, Berkeley, 1998.
19. Dabbousi, B. O.; Bawendi, M. G.; Onitsuka, O.; Rubner, M. F. *Appl. Phys. Lett*. **1995,** *66*, 1316–1318.
20. Mattoussi, H.; Radzilowski, L.; Dabbousi, B. O.; Thomas, E. L.; Bawendi, M. G.; Rubner, M. F. *J. Appl. Phys*. **1998,** *83*, 7965–7974.
21. Greenham, N. C.; Peng, X.; Alivisatos, A. P. *Phys. Rev. B* **1996,** *54*, 17628–17637.
22. Greenham, N. C.; Peng, X.; Alivisatos, A. P. *Synth. Met*. **1997,** *84*, 545–546.
23. Klein, D. L.; Roth, R.; Lim, A. K. L.; Alivisatos, A. P.; McEuen, P. L. *Nature* **1997,** *89*, 699–701.
24. Alivisatos, A. P. *MRS Bull*. **1998,** *23*, 18–23.
25. Bruchez, M. Jr.; Moronne, M.; Gin, P.; Weiss, S.; Alivisatos, A. P. *Science* **1998,** *281*, 2013–2016.
26. Chan, W. C. W.; Nie, S. *Science* **1998,** *281*, 2016–2018.
27. Rosenthal, S. J.; Tomlinson, I.; Schroeter, S.; Adkins, E.; Swafford, L.; Wang, Y.; Defelice, L.; Blakely, R. D. *J. Am. Chem. Soc*., in press.